

Synthesis of Lamellar Structures of Magnesium (II), Aluminum (III) and Iron (III) Hydroxides Interchanged with Carbonate Ion through Precipitation in pH 11

Graciele Vieira Barbosa^a, Jusinei Stropa Meirelles^b, Lincoln Carlos Silva de Oliveira^b, Rafael Aparecido Ciola Amoresi^c, Maria Aparecida Zaghete^c, Sandro Márcio Lima^a, Alberto Adriano Cavalheiro^a, Rogério Cesar de Lara da Silva^a

^aLIMAN - CDTEQ - Universidade Estadual de Mato Grosso do Sul, R. Emilio Mascoli, 275 - Jardim Vale Encantado, 79950-000, Naviraí - MS, Brazil.

^bINQUI - Universidade Federal de Mato Grosso do Sul, Av. Senador Filinto Muller, 1555 - Ipiranga, 79064-470, Campo Grande, MS, Brazil.

^cLIEC - IQCar - Universidade Estadual Paulista, Rod. Araraquara-Jaú Km, Bairro Machados, 14800-901, Araraquara, SP, Brazil.

Article history: Received: 30 June 2017; revised: 07 November 2017; accepted: 15 November 2017. Available online: 28 January 2018. DOI: <http://dx.doi.org/10.17807/orbital.v10i1.1036>

Abstract: The synthesis of layered double hydroxides has been investigated aiming in numerous applications, mainly as adsorbent, catalyst and catalyst support materials, due their ability to adsorb anionic species and several aqueous soluble compounds. The carbonated magnesium-aluminium hydroxaltes are known as the main class of the layered double hydroxides and new composition are often characterized under the view point of thermal stability, crystallinity and catalytic performance for many reactions. Few trivalent cations are able to replace the aluminum one due the severe restriction for oxidation state and ionic radii, but the iron (III) one seems to be high potential to improve some of the characteristics required for that materials, such as specificity for built-rebuilt bonds in organic molecules. In this work, we have synthesized carbonated magnesium-aluminum hydroxaltes samples through the coprecipitation at pH 11 and investigate the Fe(III) insertion at 10 and 20 mol%. Thermal analysis, FTIR spectrometry and X-ray diffractometry techniques were used to understand the influence of the Fe(III) co-substitution, keeping the Mg(II) molar fraction invariable among the samples. We show the iron (III) insertion affects the dehydration and dehydroxylation processes due the changes in M-OH bond energies. Very homogeneous structures were obtained for all of the samples dried at 100 °C and a consistent lattice volume expansion was observed as a function of iron (III) content, which can be required for catalyst or catalyst matrix applications.

Keywords: hydroxaltes; iron (III); LDH structure; precipitation; thermal analysis; X-ray diffraction

1. INTRODUCTION

Hydroxaltes are layered double hydroxides, which are classified as anionic clays due to their ability for adsorbing anionic species in interlayer spaces. The double hydroxide is based in divalent cations with Person hard acid characteristic, forming a two-dimensional plates, named lamellas, through the shared hydroxyl bonds. A charge imbalance is inserted into lamellas due the partial substitution of divalent cations by trivalent ones, which increase the ability to stabilize the interlayer species [1-5].

The application range for hydroxaltes compounds is somewhat broad and unrestricted,

taking into account their catalytic action or the enhancement of performance of others catalyst embedded into hydroxaltes matrix. There are uncountable articles demonstrating the capacity for improvement of the catalyst activity and selectivity of the hydroxaltes materials, the ability for metallic particles dispersion, and the facilities for recuperation and reuse of immobilized catalysts, due the simple and easy dissolution and re-precipitation of hydroxaltes compounds, as provided by an important review [6].

Carbonated magnesium-aluminium hydroxaltes are the most common and layered stable structures and possess the general formula given by

*Corresponding author. E-mail: grace.navi.21@gmail.com

$\text{Mg(II)}_{(1-x)}\text{Al(III)}_x(\text{OH})_2(\text{CO}_3^{-2})_{x/2}\cdot y\text{H}_2\text{O}$. Several authors have been set the x value between 0.67 and 0.8 in order to obtain a minimum of thermal stability for carbonated hydrotalcites due the importance of magnesium cation in the ordering of the octahedral sharing lamellas. In addition, at that aluminium concentration level, the interlamellar space is enough filled with systematic hydrated carbonate species, providing the lamella ordering in perpendicular direction, given a three-dimensional structure [7-11].

The Mg(II) cation in carbonated magnesium-aluminium hydrotalcites can be partially substituted by other divalent cations, such as Zn(II), Ca(II), and Co(II), making the material so different, taking into account the adsorptive characteristics. On the other hand, few trivalent cations can co-substitute the Al(III) one, usually Cr(III) and Fe(III), in spite of to have some others, like the rare earth cation Sc(III). However, the maximum level for trivalent cation substitution remains still practically unaltered, despite of the cation type, because higher charge imbalance and amount of interlayer species leads to severe structural reordering, disassembling the layer-interlayer structure in order to form any other stable structure [12-18].

There is a set of divalent and trivalent cations what can be combined to form stable hydrotalcite structures due limitations in oxidation states and ionic radii. The hexacoordinated Mg(II) have an ionic radius of 0.072 nm so that the hexacoordinated Al(III), with ionic radius of 0.054 nm [19] cause a slight lattice distortion in the lamella, originating a smoothed zigzag in surface. That geometry surface maybe is positive characteristics about the interlayer species anchorage and the thermal stability for hydrotalcite structure [20-25].

The dehydration or dehydroxylation processes can occur when the material is submitted to different operating temperatures as catalyst or catalyst matrix. The dehydration causes significant volume contraction and the pore bottlenecks, harming the catalyst performance, while the dehydroxylation one causes a complete disassembling of layered structure. However, if the material has a good structural memory, then a new ageing process by suspension of decomposed powder material in adequate pH media can recovery satisfactorily the original structure [26-34].

All of these aspects are changed by material composition and can be predict through the combination of some characterization techniques in

order to determine the water loss in each thermal event along the temperature increasing as well the mean functional groups or predominant crystalline phases. Thus, this work aims to synthesize the carbonated magnesium-aluminum hydrotalcite by hydroxide coprecipitation at pH 11 and investigate the Al(III) co-substitution with Fe(III) at 10 and 20 mol% through thermal analysis, Fourier transform infrared spectrometry and X-ray diffractometry techniques.

2. MATERIAL AND METHODS

The materials were prepared to investigate the Fe(III) co-substitution on the thermal stability and crystallinity of the hydrotalcite structures obtained after drying at 100 °C for 24 hours. Thus, the calculation step was carried out taking into account the general formula $\text{Mg(II)}_{0,7}\text{Al(III)}_{0,3-x}\text{Fe(III)}_x(\text{OH}^-)_2(\text{CO}_3^{-2})_{0,15}$, where x values was set as 0, 0.1, and 0.2. The sample designation follows the Al: Fe cation molar fractions, once Mg(II) is constant and set as 0,7. Therefore, the no Fe(III) co-substituted sample was named as HTA3C0, while the samples named as HTA2F1 HTA1F2 refer to x values set as 0.1 and 0.2, respectively.

The precipitation of hydrotalcite samples was carried out preparing two batch solutions for each composition, one of them containing a mix of cation nitrate reagents and the other containing the hydroxide and carbonate precipitating anions. The cation solution batches were prepared dissolving hexahydrate magnesium II nitrate $\text{Mg(NO}_3)_2\cdot 6\text{H}_2\text{O}$, nonahydrate aluminum III nitrate $\text{Al(NO}_3)_3\cdot 9\text{H}_2\text{O}$, and except for no Fe(III), co-substituted sample, nonahydrate iron III nitrate $(\text{Fe(NO}_3)_3\cdot 9\text{H}_2\text{O})$ in distilled water at room temperature. The anion precipitating solutions was prepared dissolving simultaneously sodium hydroxide (NaOH) and sodium carbonate (Na_2CO_3) with distilled water at room temperature too. The final volume for both solutions was adjusted in order to set the total cation molarity to 0.1 molar during the precipitation, which was executed by pouring both solution in a third flask under vigorous stirring at room temperature. After the ageing stage at 80 °C for 6 hours under moderate stirring, the precipitate suspensions were finally caped and rested overnight at room temperature before the purification process.

Each batch precipitate suspension was filtered several times with distilled water until the filtered solution to present a neutral pH and lead to drying

process at 85 °C for 24 hours, soft milling to reduce the agglomerates and finally dried again at 100 °C again for 24 hours in conventional drying oven. The samples were characterized by simultaneous Thermal Analysis (TG/DSC) by using a Netzsch - Thermische Analyze equipment, with TASC 414/2 controller and Pt 10 thermocouple, under synthetic air flow of 30 mL min⁻¹ and heating rate of 10 °C min⁻¹.

They were also characterized by Fourier Transform Infrared (FTIR) spectrometry using Nexus 650 Thermo Nicolet equipped with photoacoustic detector and the main functional groups identified according the literature [35,36]. Finally, the samples were characterized by X-ray diffractometry using Siemens equipment, model D5005 (K-alpha-Cu radiation) and the x-ray diffraction pattern was analyzed by comparing the most intense peaks with similar structure available on the JCPDS database [37].

3. RESULTS AND DISCUSSION

Thermal events for dried hydrotalcite precipitates were evaluated through simultaneous TGA/DSC techniques, as shown in Figure 1. No co-substituted sample HTA3F0 (Fig. 1.a) show the decomposition of dried precipitate occurs in three distinguishable stages, according DTG peaks. It is possible to observe the DTG peaks are very coherent with DSC ones, what means those weight loss have specific thermodynamic behaviors for dehydration and dehydroxylation stages. However, above 450 °C, a kinetic weight loss can be observed, which extends up to 900 °C, indicating the decarbonation process is mainly overlapping with final dehydroxylation one.

Different from the HTA3F0 sample, which presents a left side shoulder for the first weight loss (I), the HTA2F1 and HTA1F2 samples present that weight loss displaced to lower temperature in overlapping with possible left side shoulder existent. In previous work, an accurate study about the several water loss stages was examined through mass spectroscopy of the gaseous products and the results were compared to DTG and DTA peaks for each decomposition stage [38]. The left shoulder observed for HTA3F0 sample is related to dehydration of the external surface adsorbed water, while the main peak close to 200 °C refers to desorption of interlayer water molecules.

In Table 1 are shown the weight loss for each thermal event obtained from TG/DSC curves and it is

possible to observe the desorbed water amount are very close among the samples. Thus, maybe the iron (III) co-substituted samples possess more amounts of external surface adsorbed water due the differences in tridimensional ordering of the lamellas or even the interlayer spaces are larger than the one occurring in HTA3F0 sample, which eases the water molecule desorption. Nevertheless, both hypotheses are until now indistinguishable, taking into account only the thermal studies.

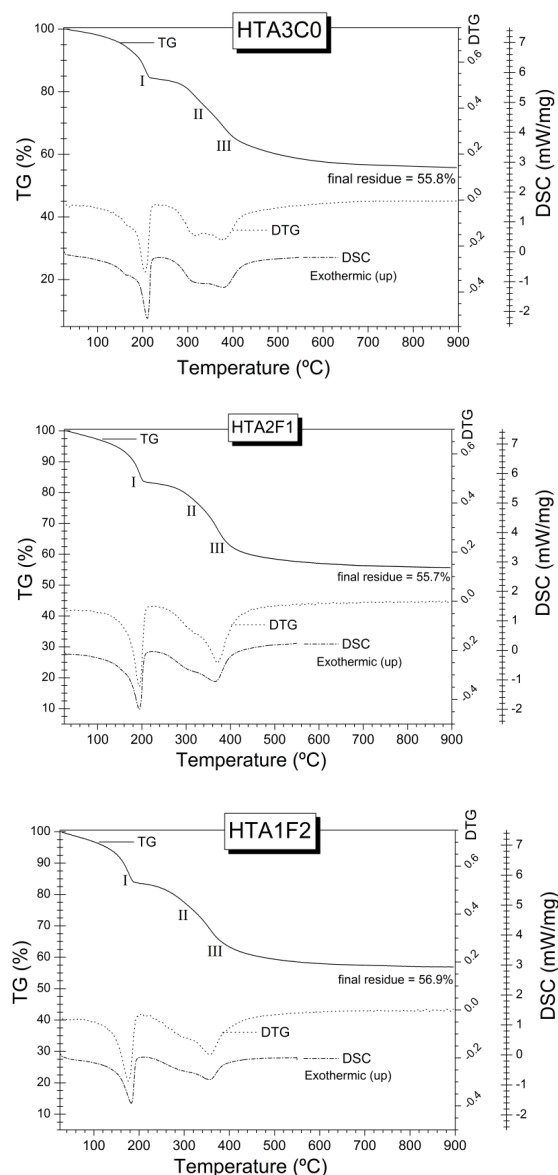


Figure 1. Thermal analysis (TG/DTG/DSC) for carbonated magnesium-aluminum precipitates dried at 100 °C, as a function of Fe(III) content: a) HTA3F0, b) HTA2F1 and c) HTA1F2 samples.

The second and third thermal events are associated to the dehydroxylation and extend up to

450 °C. These two water loss events indicate the short differences among the hydroxyl groups in lamellae surface. Taking into account the hydroxyl groups are shared by the octahedron edges, the presence of divalent or trivalent cations in one or more vicinal octahedron can change the bond energy of the hydroxyl groups in lamellae surface and these aspects were also inferred in above mentioned work [38]. Also, the aluminium hydroxide is more easily dehydroxylated (290 °C) than iron(III) one (350 °C), which would make the iron(III)-based hydrotalcites more difficultly dehydroxylated [39].

Nevertheless, according the results presented in a third work, is very probable that both hypotheses are not true, because the temperature of dehydroxylation process for crystalline metallic hydroxides is not only dependent of M-OH bond energies but is also dependent of the mechanism of water loss from different localization in layer-interlayered structure. In the last instance, the differences for DTG peaks and tabled weight loss presented in present work, shows the both dehydroxylation stages (II and III) tends to be higher for higher contents of Fe(III). There two possible causes for those results, which is related to carbonate

amount in interlayer space. One of them, is based less amounts of carbonate for higher Fe(III) content samples, which eases the dehydroxylation process. The other is the overlapping in decarbonation process before the second dehydroxylation process has been finished. Both causes can explain the decreasing in decarbonation process between 500 and 900 °C and save also a direct relationship with observable differences for ordering process.

The FTIR spectra for all of the samples are shown in Figure 2. At 3500 cm⁻¹ (I) and 3000 cm⁻¹ (II) are observed the stretching vibration of -OH groups from interlayer water and metal hydroxides, respectively. The band II appears displaced to lower wavenumber as a function of Fe(III) content and is also dismembered in two shaper and low intense bands, which shows to have energetic differences for M-OH bonds caused by Fe(II) insertion. At 2350 cm⁻¹ (III) appears the band associated to the adsorbed CO₂, which seems constant among the samples and is probably originated from ambient atmosphere during the analysis, because at 1650 cm⁻¹ (IV), 1540 cm⁻¹ (V), and 1360 cm⁻¹ (VI) there are the bands associated to interlayer hydrated carbonate ions.

Table 1. Thermal events for carbonated magnesium-aluminum hydrotalcite dried at 100 °C for 24 h.

Thermal event	I Water Loss (%)	II Water Loss (%)	III Water Loss (%)	Carbon dioxide loss (%)	Final Residue (%)
Temperature	up to 230 °C	from 230 to 320 °C	from 320 to 500 °C	from 500 to 900 °C	at 900 °C
HTA3F0	16.8	7.9	14.4	5.1	55.8
HTA2F1	17.0	8.4	15.1	3.8	55.7
HTA1F2	17.1	8.7	15.8	1.5	56.9

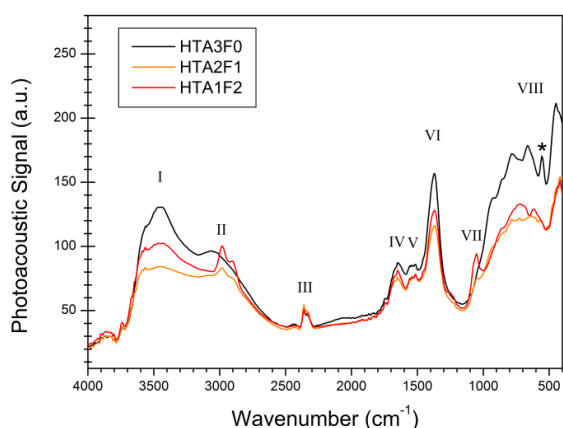


Figure 2. FTIR spectra for the carbonated magnesium-aluminum precipitate samples dried at 100 °C.

At 1100 cm⁻¹ (VII) is observed the band

associated to hydroxide layer structure originated from M-OH translation mode, which seems to be directly influenced by Fe(III) content. An opposite change occurs for the band at 555 cm⁻¹ (*), localized among a set of bands (VIII) below 900 cm⁻¹, which are related to the M1-O-M2 vibration modes. In the time the band VII increases as a function of Fe(III) content, the band at 555 cm⁻¹ (*) decreases, which seems to be a dependent behavior of the trivalent cation sites.

In Figure 3 is shown the X-ray diffraction patterns for all of the hydrotalcite samples, where it is possible to observe the R-3m rhombohedral phase as a single phase in the precipitate samples, despite of the iron insertion, according the card number 89-5434 of the JCPDS data bank for powder diffraction patterns. No residual nitratine NaNO₃ phase was found, which implicates the washing stage was

successfully carried out for all of the samples. It is possible the structural rearrangement of rhombohedral hydrotalcite into another rhombohedral phase containing magnesium and iron (III) hydroxide carbonate, like the piroaurita $\text{Fe}_{0.25}\text{Mg}_{0.75}(\text{OH})_2(\text{CO}_3)_{0.125}(\text{H}_2\text{O})_{0.56}$, according JCPDS card number 70-2150.

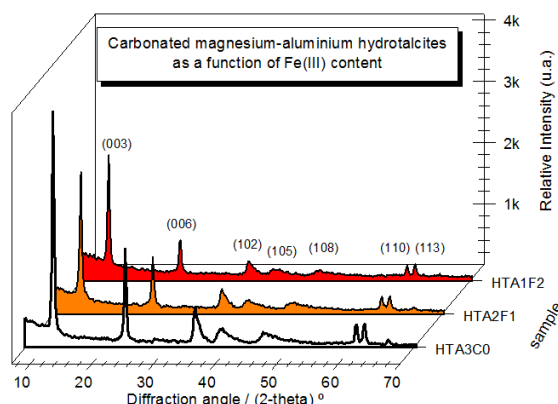


Figure 3. X-ray diffraction patterns for the carbonated magnesium-aluminum precipitate samples dried at 100 °C.

By comparing the peak positions for both structures, it is possible to observe the peak position related to the (110) and (113) reflections for hydrotalcite structure present a noticeable and continuous displacement for to lower 2-theta angles as a function of the Fe(II) content, in similar way to the expected for piroaurita structure, as can be view in Figure 4, referent to crop region at high X-ray diffraction angle. However, it not probable the

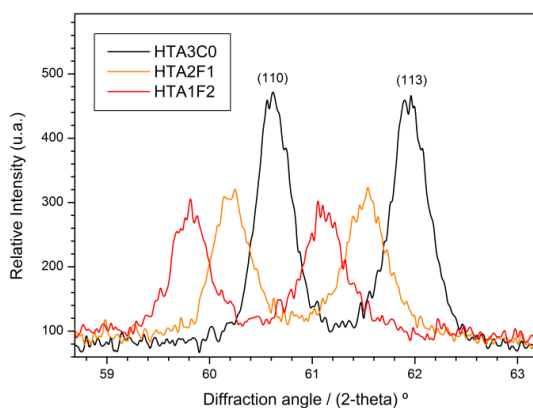


Figure 4. Crop region at high X-ray diffraction angle, showing the peak displacement of (110) and (113) reflections to lower 2-theta angles as a function of Fe(III) content.

occurrence of that secondary phase containing high amount of iron (III) in the HTA2F1 and HTA1F2

samples, because the full width at half maximum (FWHM) values for both peaks related to (110) and (113) reflections stay constant in 0.4 and 0.5 °, respectively. That observation permits to infer the iron (III) is inserted in hydrotalcite structure with compositional and structural homogeneity, which is coherent with ionic radii differences between hexacoordinated Al(III) (0.054 nm) and Fe(III) (0.065 nm) cations, once bigger cation tends to expand the unit cell, which displaces the peak position to lower diffraction angle, according Bragg's Law.

4. CONCLUSION

In this work we present some results about the synthesis and characterization of carbonated magnesium-aluminum hydrotalcites obtained by precipitation method at pH 11. The results were discussed taking into account the influence of the Fe(III) co-substitution, keeping the Mg(II) molar fraction invariable among the samples. It was possible to observe the iron (III) insertion affects the dehydration and dehydroxylation processes due the differences in carbonate anchorage into lamellar spaces. FTIR spectroscopy showed that bond energies for M-OH groups are changed with iron insertion and the X-ray diffractometry showed that a very homogeneous structure was obtained, with a consistent lattice variation. Thus, that satisfactorily stable structure is able to be applied as catalyst or catalyst matrix, in special for reaction susceptible to presence of iron (III) presence.

5. ACKNOWLEDGMENTS

The authors thank FUNDECT-MS, CNPq, CAPES and FINEP for financial supports.

6. REFERENCES AND NOTES

- [1] Yang, Y.; Gao, N.; Chu, W.; Zhang, Y.; Ma, Y. *J. Haz. Mater.* **2012**, *209*, 318. [\[CrossRef\]](#)
- [2] Nguyen, H. K. D.; Nguyen, T. D.; Hoang, D. N.; Dao, D. S.; Nguyen, T. T.; Wanwisa, L.; Hoang, L. L. *Korean J. Chem. Eng.* **2017**, *34*, 314. [\[CrossRef\]](#)
- [3] Fahami, A.; Al-Hazmib, F. S.; Al-Ghamdib, A.; Mahmoudb, W. E.; Beall, G. W. *J. Alloys Compd.* **2016**, *683*. [\[CrossRef\]](#)
- [4] Tsai, T.-Y.; Laiob, J.-R.; Naveen, B. *J. Chin. Chem. Soc.* **2015**, *62*, 547. [\[CrossRef\]](#)
- [5] Bhat, B. M. *Orient. J. Chem.* **2012**, *28*, 1751. [\[CrossRef\]](#)
- [6] Sels, B. F.; De Vos, D. E.; Jacobs, P. A. *Cat. Rev. - Sci.*

- Eng.* **2001**, *43*, 443. [\[CrossRef\]](#)
- [7] Ma, W.; Zhao, N.; Yang, G.; Tian, L.; Wang, R. *Desalination* **2011**, *268*, 20. [\[CrossRef\]](#)
- [8] Crepaldi, E. L.; Valim, J. B. *Quim. Nova* **1998**, *21*, 300. [\[CrossRef\]](#)
- [9] Hafshah, H.; Prajitno, D. H.; Roesyadi, A. *Bull. Chem. React. Eng. Catal.* **2017**, *12*, 273. [\[CrossRef\]](#)
- [10] Niu, M.; Qiu, M.; Han, Q.; Wang, Y. *Am. Chem. Sci. J.* **2016**, *15*, 1. [\[CrossRef\]](#)
- [11] Fahami, A.; Beall, G. W. *J. Solid State Chem.* **2016**, *233*, 422. [\[CrossRef\]](#)
- [12] Bhanawase, S. L.; Yadav, G. D. *Ind. Eng. Chem. Res.* **2017**, *56*, 12899. [\[CrossRef\]](#)
- [13] Velu, S.; Swamy, C. S. *Appl. Catal., A* **1997**, *162*, 81. [\[CrossRef\]](#).
- [14] Lung, Y.-F.; Sun, Y.-S.; Lin, C.-K.; Uan, J.-Y.; Huang, H.-H. *Scientific Reports* **2016**, *6*, 32458. [\[CrossRef\]](#)
- [15] Islam, M. R.; Guo, Z.; Rutmana, D.; Benson, T. J. *RSC Adv.* **2013**, *3*, 24247. [\[CrossRef\]](#)
- [16] Carpani, I.; Berrettoni, M.; Giorgetti, M.; Tonelli, D. *J. Phys. Chem. B* **2006**, *110*, 7265. [\[CrossRef\]](#)
- [17] Del Arco, M.; Malet, P.; Trujillano, R.; Rives, V. *Chem. Mater.* **1999**, *11*, 624. [\[CrossRef\]](#)
- [18] Mahjoubia, F. Z.; Khalidib, A.; Abdennouria, M.; Barkaa, N. *Desalination Water Treat.* **2015**, *1*. [\[CrossRef\]](#)
- [19] Shannon, R. D. *Acta Cryst.* **1976**, *A32*, 751. [\[CrossRef\]](#)
- [20] Jatav, J.; Jatav, R.; Bhardwaj, S. K.; Sahu, P. K.; Kumar, K. *J. Chem. Pharm. Res.* **2016**, *8*, 678. [\[CrossRef\]](#)
- [21] Li, J.-G.; Ikegami, T.; Lee, J.-H.; Mori, T. *J. Am. Ceram. Soc.* **2000**, *83*, 2866. [\[CrossRef\]](#)
- [22] Timofeevaa, M. N.; Kapustinc, A. E.; Panchenkoa, V. N.; Butenkoc, E. O.; Krupskayad, V. V.; Gil, A.; Vicenteg, M. A. *J. Mol. Catal. A: Chem.* **2016**, *423*, 22. [\[CrossRef\]](#)
- [23] Carpentier, J.; Siffert, S.; Lamonier, J. F.; Laversin, H.; Aboukais, A. *J. Porous Mater.* **2007**, *14*, 103. [\[CrossRef\]](#)
- [24] Debek, R.; Motak, M.; Galvez, M. E.; Grzybek, T.; Da Costa, P.; Pieńkowski, L. *E3S Web of Conferences* **2017**, *14*, 02039. [\[CrossRef\]](#)
- [25] Balcomb, B.; Singh, M.; Singh, S. *Chemistry Open* **2015**, *4*, 137. [\[CrossRef\]](#)
- [26] Ogata, F.; Kawasaki, N. *Chem. Pharm. Bull.* **2015**, *63*, 1040. [\[CrossRef\]](#)
- [27] Ardhayanti, L. I.; Santosa, S. J. *Procedia Eng.* **2016**, *148*, 1380. [\[CrossRef\]](#)
- [28] Sani, T.; Adem, M.; Fetter, G.; Bosch, P.; Diaz, I. *Water Air Soil Pollut.* **2016**, *227*, 2. [\[CrossRef\]](#)
- [29] Ríos, E.; Hernández, M.; Ibarra, I. A.; Guzmán, A.; Lima, E. *Chem. Cent. J.* **2016**, *10*, 1. [\[CrossRef\]](#)
- [30] Volli, V.; Purkait, M. K. *Clean Technol. Environ. Policy* **2016**, *18*, 529. [\[CrossRef\]](#)
- [31] Toledo, T. V.; Bellato, C. R.; Pessoa, K. D.; Fontes, M. P. F. *Quim. Nova* **2013**, *36*, 419. [\[CrossRef\]](#)
- [32] Zhou, W. Y.; Pan, J. G.; Wu, Z.; Qian, J. F.; He, M. Y.; Chen, Q. *RSC Adv.* **2016**, *6*, 84106. [\[CrossRef\]](#)
- [33] Navajas, A.; Campo, I.; Arzamendi, G.; Hernández, W. Y.; Bobadilla, L. F.; Centeno, M. A.; Odriozola, J. A.; Gandía, L. M. *Appl. Catal., B* **2010**, *100*, 299. [\[CrossRef\]](#)
- [34] Miranda, L. D. L.; Bellato, C. R.; Milagres, J. L.; Moura, L. G.; Munteer, A. H.; de Almeida, M. F. *J. Environ. Manage.* **2015**, *156*, 225. [\[CrossRef\]](#)
- [35] Lopez, T.; Bosch, P.; Asomoza, M.; Gomez, R.; Ramos, E. *Mater. Lett.* **1997**, *31*, 311. [\[CrossRef\]](#)
- [36] Socrates, G. *Infrared and Raman Characteristic Group frequencies*, 3th ed., John Wiley & Sons, Chichester, 2004. [\[CrossRef\]](#)
- [37] JCPDS - Joint Committee on Powder Diffraction Standards/International Center for Diffraction Data, Pennsylvania, Powder Diffraction File 2003.
- [38] Zhang, J.; Xu, Y.F.; Qian, G.; Xu, Z. P.; Chen, C.; Liu, Q. *J. Phys. Chem. C* **2010**, *114*, 10768. [\[CrossRef\]](#)
- [39] Yang, W. Kim, Y.; Liu, P. K. T.; Sahimi, M.; Tsotsis, T. T. *Chem. Eng. Sci.* **2002**, *57*, 2945. [\[CrossRef\]](#)